Downward transport of upper atmospheric NO_x into the polar stratosphere and lower mesosphere during the Antarctic 2003 and Arctic 2002/2003 winters

B. Funke, M. López-Puertas, and S. Gil-López
Instituto de Astrofísica de Andalucía, Consejo Superior de Investigaciones Cientificas, Granada, Spain

T. von Clarmann, G. P. Stiller, H. Fischer, and S. Kellmann
Institut für Meteorologie und Klimaforschung, Forschungszentrum Karlsruhe und Universität Karlsruhe, Karlsruhe, Germany

Received 4 July 2005; revised 12 September 2005; accepted 10 October 2005; published 28 December 2005.

[1] Pronounced upper stratospheric and mesospheric NO_x enhancements were measured by the Michelson Interferometer for Passive Atmospheric Sounding (MIPAS) in the Southern Hemisphere (SH) polar vortex from May to August 2003, reaching average abundances of 60 ppbv at 50–60 km in July. Peak mixing ratios of around 200 ppbv were measured in the polar night, representing the highest values ever recorded in the SH. The observed NO_x enhancements are attributed to production by electron precipitation in the upper mesosphere and lower thermosphere and subsequent descent with the meridional circulation. Using measured CH_4 and CO distributions as dynamic tracers, the downward transport of NO_x-rich air masses into the lower and middle stratosphere has been investigated. Upper atmospheric air with average NO_x abundances of 15 ppbv reached the 800–1000 K potential temperature region (around 30 km) by the end of July, where it remained until the final warming in late October. The NO_x descent was confined to the polar vortex, although significant mixing of tropical and NO_x-rich vortex air masses began already in August above 40 km. The amount of upper atmospheric NO_y measured inside of the SH vortex in late spring was 1.1 Gigamoles (GM) which is in good agreement with previous estimates from HALOE data. The global coverage of MIPAS data further allows to quantify the upper atmospheric NO_x dispersed into the stratosphere during August-September, estimated in 1.3 GM. The net deposition of NO_x into the stratosphere during the 2003 Antarctic winter (2.4 GM) makes up 9% of the N_2O oxidation source in the SH, twice as much as estimated in previous studies. NO_x and tracer distributions observed on several days during the NH winter 2002/2003 have been analyzed for comparison. We found that high planetary wave activity, resulting in the major midwinter warming had led to a rather inefficient NO_x downward transport with negligible deposition of NO_x into the lower and middle stratosphere.

Citation: Funke, B., M. López-Puertas, S. Gil-López, T. von Clarmann, G. P. Stiller, H. Fischer, and S. Kellmann (2005), Downward transport of upper atmospheric NO_x into the polar stratosphere and lower mesosphere during the Antarctic 2003 and Arctic 2002/2003 winters, *J. Geophys. Res.*, *110*, D24308, doi:10.1029/2005JD006463.

1. Introduction

[2] Nitrogen oxides, $NO_x = NO + NO_2$, are the major drivers of catalytic ozone loss in the middle stratosphere. In this altitude region, NO_x forms a pronounced layer peaking around 35–40 km with volume mixing ratios (VMRs) of typically 10–17 ppbv. The major chemical source for stratospheric NO_x is oxidation of N_2O injected from the troposphere in the tropics. A second NO_x layer exists in the thermosphere and is produced by dissociation of molecular nitrogen by solar photons and energetic particles, in particular auroral and precipitating electrons from the outer trapping region of the magnetosphere, and subsequent reaction of $N(^4S,^2D)$ with oxygen to form NO. Depending on solar and geomagnetic activity, maximum thermospheric NO VMRs can vary from 100 up to 2000 ppmv, which, in terms of number densities, becomes comparable to stratospheric NO_x abundances. Both stratospheric and thermospheric NO_x layers are normally separated by a mesospheric minimum caused by reactions

$$NO + h\nu \rightarrow N + O \tag{R1}$$

$$NO + N \rightarrow N_2 + O \tag{R2}$$

0148-0227/05/2005JD006463$09.00

which reduce the chemical lifetime of NO to only a few days.

[3] In the absence of sunlight during polar winter, however, large amounts of upper atmospheric NO_x can be transported down to the mesosphere and stratosphere by the meridional circulation without being photochemically destroyed. This mechanism was already proposed by *Solomon et al.* [1982] and *Frederick and Orsini* [1982]. Once transported down to the stratosphere, NO_x is photochemically stable and may thus contribute to the stratospheric NO_y budget and hence to the global O_3 variability [*Siskind*, 2000]. Enhanced upper stratospheric and mesospheric NO_2 reaching levels of about 175 ppbv at 70 km at polar night conditions was measured by the Limb Infrared Monitor of the Stratosphere (LIMS) instrument [*Russell et al.*, 1988] during the 1978/1979 winter in the Northern Hemisphere (NH), representing the first experimental evidence for downward transport of thermospheric NO_x. By correlating CH_4, NO, and NO_2 measured by the Halogen Occultation Experiment (HALOE) experiment on the Upper Atmospheric Research Satellite (UARS), *Siskind et al.* [2000] clearly demonstrated the existence of NO_x-rich upper atmospheric air in the Southern Hemisphere (SH) polar winter stratosphere during 1992–1996. Similar observations were made by the Atmospheric Trace Molecule Spectroscopy (ATMOS) experiment [*Rinsland et al.*, 1999] and the Polar Ozone and Aerosol Measurement (POAM II) Instrument [*Randall et al.*, 1998] for different NH and SH winters. All measurements suggest that the NO_x descent is well confined within the polar vortex. In various model studies and comparisons to NO_x data from HALOE and the Stratospheric Aerosol and Gas experiment (SAGE II), *Callis et al.* [1998a, 1998b, 2001, 2002] investigated the role of electron precipitation from the outer trapping region of the magnetosphere as observed aboard TIROS spacecraft on the polar winter descent of NO_x. They identified this production mechanism as the dominant NO_x source in the polar upper atmosphere and found a significant modulation of stratospheric NO_y and O_3 by electron precipitation within the solar cycle. *Randall et al.* [1998] and *Siskind et al.* [2000] have shown that interannual variations of the NO_x enhancements in the polar winter stratosphere are closely linked to variations of the geomagnetic A_p index, suggesting that NO_x downward transport is predominantly controlled by the upper atmospheric source rather than by dynamical conditions. On the other hand, a pronounced hemispherical asymmetry was found in NO_x HALOE observations, with larger polar winter enhancements occurring in the SH [*Siskind*, 2000]. This hemispheric asymmetry could be reproduced by 2-D chemical transport model (CTM) calculations when including a larger gravity wave drag in the SH and enhanced planetary wave forcing in the NH which demonstrates the important role of dynamics [*Siskind et al.*, 1997]. However, the CTM model failed to reproduce mesospheric NO enhancements measured by HALOE at latitudes as far equatorward as 30°–40° and it overestimated the net deposition of NO_x in the stratosphere. Both limitations were attributed to an underestimation of horizontal mixing in the lower mesosphere. Thus, despite the numerous measurements confirming the downward transport of NO_x in polar winter, the overall understanding of its mechanism is limited by the lack of NO_x data poleward of 50° along the whole winter [*Siskind*, 2000].

[4] A local source of mesospheric and upper stratospheric NO_x is highly energetic solar protons (>1 MeV) ejected during strong solar storms and penetrating into the Earth's middle atmosphere in the polar regions. During the July 2000 SPE, NO_x enhancements of 50–100 ppbv were detected by HALOE at 65–70°N in the 55–70 km altitude range [*Jackman et al.*, 2001]. In October and November 2003, an unusually powerful solar proton event (SPE) led to local NO_x enhancements reaching 180 ppbv in the North polar upper stratosphere as measured by the Michelson Interferometer for Passive Atmospheric Sounding (MIPAS) experiment [*López-Puertas et al.*, 2005]. In principle, SPE-induced NO_x production takes place in both hemispheres with a similar magnitude. However, the impact on stratospheric ozone chemistry is more severe in the winter hemisphere because of the longer photochemical lifetime of NO_x and favorable dynamical conditions. *López-Puertas et al.* [2005] have reported significant NO_x-induced O_3 depletion after the October-November 2003 SPE in the North polar stratosphere while in the Austral polar regions changes in O_3 and NO_x disappeared within a few days.

[5] In situ production of lower mesospheric and upper stratospheric NO_x is also possible by precipitating electrons from the outer trapping region with energies larger than 100 keV. *Callis and Lambeth* [1998] reported NO_2 enhancements of up to 140 ppbv around 60 km during the 1991 NH winter and the 1992 SH winter which had been attributed to such electron events.

[6] The Michelson Interferometer for Passive Atmospheric Sounding (MIPAS) [*Fischer and Oelhaf*, 1996; *European Space Agency*, 2000] measures both NO_x constituents, NO and NO_2, as well as the dynamical tracers CH_4 and CO with global coverage and independent of illumination conditions. It is thus perfectly suited for studying polar winter NO_x enhancements in the mesosphere and upper stratosphere and its downward transport. Here, we analyze MIPAS measurements regarding NO_x, CH_4, and CO covering the winter poles between September 2002 and October 2003. In the Antarctic winter 2003, strong NO_x enhancements were observed which were larger than ever reported in the SH. In this study, we focus on this winter in order to assess the deposition of upper atmospheric NO_x into the stratosphere.

[7] In section 2, MIPAS observations and the data analysis method are described. In section 3, we discuss the NO_x and tracer distributions observed during the Antarctic winter 2003. Possible NO_x production mechanisms are assessed in section 4. The modulation of the NO_x descent by atmospheric dynamics is discussed in section 5. A quantitative estimation of the stratospheric deposition of upper atmospheric NO_x is given in section 6. Finally, we compare the observed NO_x descent in the Austral winter 2003 with the Arctic winter 2002/2003 in section 7.

2. MIPAS Observations and Data Analysis

[8] MIPAS is a limb emission Fourier transform spectrometer operating in the midinfrared spectral region. It has been designed for measurement of atmospheric trace species from space [*European Space Agency*, 2000; *Fischer and Oelhaf*, 1996]. It is part of the instrumentation of the

Table 1. Temporal Coverage of Available IMK/IAA Data

Day	Number of Orbits	Number of Observations
16 Nov. 2002	8	578
24 Nov. 2002	9	624
1 Jan. 2003	9	537
11 Jan. 2003	7	485
26 Jan. 2003	6	374
18 Feb. 2003	9	698
30 Mar. 2003	9	683
11 Apr. 2003	9	479
19 Apr. 2003	10	487
29 Apr. 2003	9	571
11 May 2003	10	645
17 May 2003	10	577
23 May 2003	10	593
6 June 2003	10	722
9 June 2003	10	721
20 June 2003	10	648
1 July 2003	10	711
11 July 2003	10	642
21 July 2003	10	576
1 Aug. 2003	10	722
11 Aug. 2003	10	721
21 Aug. 2003	10	659
31 Aug. 2003	10	702
22 Sep. 2003	10	724
30 Sep. 2003	10	708
10 Oct. 2003	9	708

Environmental Satellite (ENVISAT) which was launched into its Sun-synchronous polar orbit of 98.55° inclination at about 800 km altitude on 1 March 2002. MIPAS operated from July 2002 to March 2004 at full spectral resolution of 0.05 cm^{-1} in terms of full width at half maximum (apodized with the strong *Norton and Beer* [1976] function). MIPAS observes the atmosphere during day and night with global coverage from pole to pole and thus provides trace gas distributions also during polar night. Within its standard observation mode, MIPAS covered the altitude range from 6 to 68 km with tangent altitudes from 6 to 42 km every 3 km, and further tangent altitudes at 47, 52, 60, and 68 km. MIPAS passes the equator in southerly direction at 10.00 am local time 14.3 times a day. During each orbit up to 72 limb scans are recorded. The Level-1b processing of the data, including processing from raw data to calibrated phase-corrected and geolocated radiance spectra, is performed by the European Space Agency (ESA) [*Nett et al.*, 1999].

[9] Data presented and discussed in this paper are vertical profiles of abundances of NO_2, NO, CH_4 and CO, which were retrieved with the dedicated scientific IMK-IAA data processor [*von Clarmann et al.*, 2003a, 2003b] from spectra (versions 4.55 to 4.59) recorded from November 2002 to October 2003. The temporal coverage of observations analyzed in this study are summarized in Table 1. Retrieval strategies considering nonlocal thermodynamic equilibrium (non-LTE) effects, error budget and altitude resolution for the species under investigation are reported by *Funke et al.* [2005] for NO and NO_2, *Funke et al.* [2001, 2003] for CO, and *Glatthor et al.* [2005] for CH_4. The estimated precision in terms of the quadratic sum of all random errors is better than 1 ppbv for NO, at an altitude resolution of 4–7 km. The accuracy, derived by quadratically adding the errors due to uncertainties in spectroscopic data, temperature, non-LTE related parameters, and horizontal gradients to the measurement noise error, varies between 0.6 and 1.8 ppbv. The precision, accuracy, and altitude resolution of the NO_2 retrieval is estimated at 0.2–0.3 ppbv, 0.3–1.5 ppbv, and 3.5–6.5 km, respectively. For CO, precision, accuracy, and altitude resolution are 0.01–0.1 ppmv, 0.03–0.2 ppmv, and 4–15 km, respectively, and for CH_4 0.015–0.14 ppmv, 0.11–0.24 ppmv, and 3–5 km, respectively.

[10] Since these episode-based scientific MIPAS-IMK-IAA data are available only for selected periods, we have also included the operational ESA NO_2 and CH_4 data (reprocessed data version 4.61/4.62) in our analysis. ESA data are retrieved with the operational retrieval algorithm as described by *Ridolfi et al.* [2000] and *Carli et al.* [2004]. These operational MIPAS data include neither NO nor CO; further, effects due to non-LTE are ignored in the retrieval of NO_2 there.

[11] In order to analyze the retrieved trace gas profiles in a dynamical context, potential vorticity data from ECMWF analysis has been used. The operational ECMWF medium-range forecasting system is based on a global atmospheric model with comprehensive parameterizations of physical processes, tightly coupled with an ocean wave model. Variables are represented at 60 levels in the vertical, ranging from the ground 0.1 hPa (around 65 km). Incremental four-dimensional variational data assimilation (4D-Var) is used to produce initial conditions, on the basis of in situ and remotely sensed observations of temperature and winds.

[12] Whenever the boundary of the polar vortex was relevant to our analysis, we have applied the vortex boundary criterion suggested by *Nash et al.* [1996] modified such that, the second indicator besides potential vorticity, was the first derivative of a horizontal tracer distribution instead of the wind field. Above the 2000 K potential temperature level we have used the CO field, while CH_4 was used below.

3. Temporal Evolution of NO_x and Tracer Distributions

[13] A comprehensive picture of the observed NO_x descent during Antarctic winter 2003 can be gained from the MIPAS NO_2 and CH_4 ESA operational data with quasi-continuous temporal coverage. Because of the rapid conversion of NO into NO_2 in the absence of sunlight, nighttime NO_2 is a reasonable proxy for total NO_x. However, it should be noted that because of the neglect of non-LTE effects in ESA processing, their NO_2 VMRs might be underestimated by up to 30% above 50 km [*Funke et al.*, 2005]. Figure 1 (top) shows nighttime NO_2 abundances at potential temperatures between 625 K and 3000 K (approximately 25–60 km) averaged on a daily basis within 60–90°S equivalent latitudes representing roughly the polar vortex in the March–November 2003 period. The NO_2 enhancement appeared at 3000 K in early May. It reached its maximum of 60 ppbv around 1 July. NO_2 then decreased continuously until it disappeared at the beginning of September. At lower altitudes, the enhancements appeared later and with damped intensity. Finally, a tongue of enhanced NO_2 reaches the 700–800 K level by the end of September. The observed NO_2 enhancements are correlated in time and altitude with decreased CH_4 abundances (Figure 1, bottom) confirming that the enhanced NO_2 was descending from the

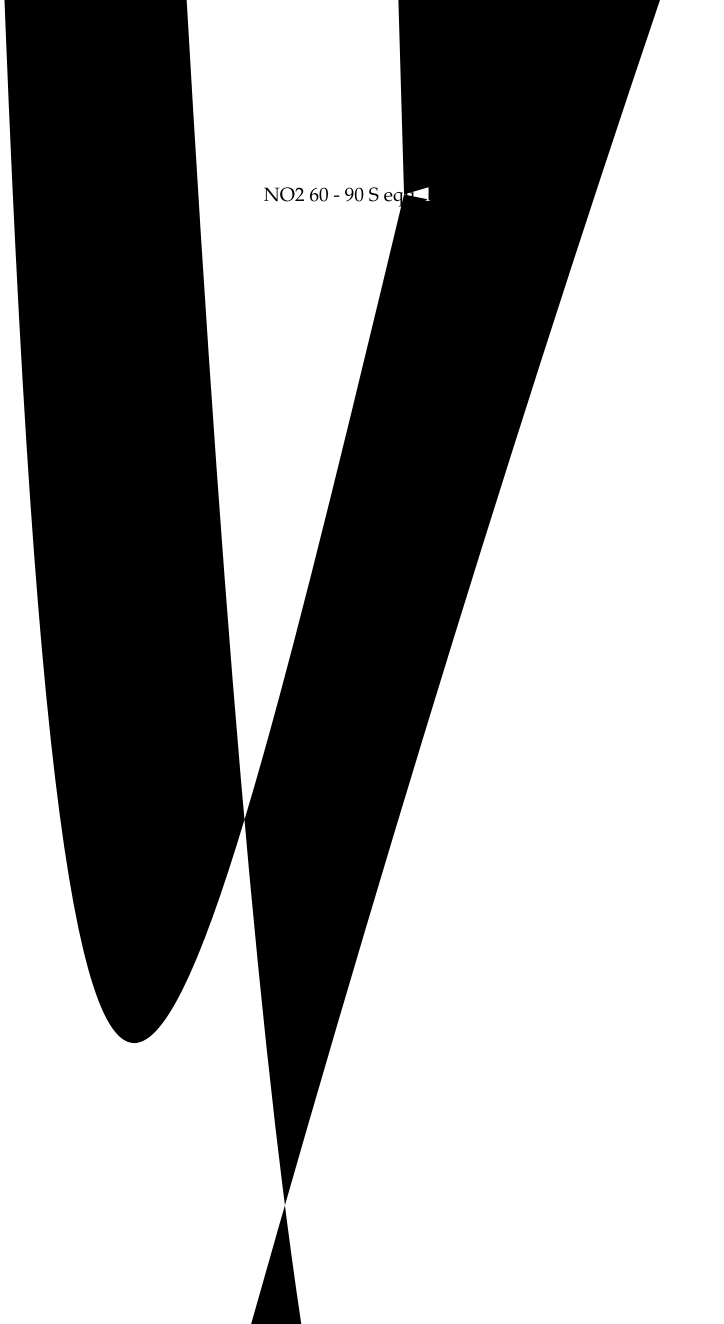

upper atmosph[illegible] However, the CH_4 decrease above 2500 K started [illegible]y in April while NO_2 began to build up in May. Thi[illegible] was caused by efficient photochemical loss of N[illegible]pril when the polar night area was still small. B[illegible] region of subsiding air with low CH_4 concen[illegible] tongue of enhanced CH_4 can be seen, localiz[illegible]00 K in March and descending to 1200 K in [illegible]H_4 enhancements were generated by an acc[illegible]-Dobson circulation with strong poleward [illegible]titudinal air masses rich in CH_4 preceding [illegible]otion. In August, CH_4 abundances s[illegible]ove 1500 K, indicating that isentrop[illegible]polar region augmented in the upper s[illegible]esosphere, probably at the same time w[illegible] began to weaken. The increas[illegible] CH_4 in A[illegible]t along with a pron[illegible] NO_2. The s[illegible] increase of [illegible] in mid-Octo[illegible] the pola[illegible] vortex ruptur[illegible] filled with midlatitude air masses rich in CH_4 and NO_2. Thus the NO_2 increase after 15 October around 1000 K is not related to upper atmospheric NO_x. The instantaneous NO_2 enhancement on 29 October at the right border of Figure 1 (top) was produced by the major SPE discussed in detail by *López-Puertas et al.* [2005].

[14] NO_x and tracer distributions have been analyzed in more detail using the IMK/IAA data of NO, NO_2, CO, and CH_4 for the available days during Antarctic winter 2003. Since the efficiency of NO_x downward transport depends on the extension and permeability of the polar vortex, the vortex boundaries have been determined from the ECMWF potential vorticity together with measured CH_4 and CO distributions, as described in section 2. Given that the temperature and wind measurements in the upper stratosphere assimilated in the ECMWF model are sparse, ECMWF wind and potential vorticity data represent an unverified forecast. Therefore consistency of these data has been checked with the measured tracer distributions. As an example, measured CO and CH_4 abundances and potential vorticity along equivalent latitude are shown in Figure 2 at the 2750 K isentrope for days 23 May, 9 June, and 21 August 2003. Pronounced horizontal gradients of all quantities can be seen at the vortex boundary close to 35°S in May and June, indicating a strong and isolated vortex. In the tracer distributions, there is no hint at transport out of the vortex. This changed in August, when horizontal gradients in the tracer abundances and potential vorticity were weak. There is evidence of mixing across the vortex boundary, then. This is in agreement with the temporal evolution of CH_4 ESA data (Figure 1), showing a CH_4 increase in August above 1500 K in the polar region. Also, the temporal evolution of the ECMWF zonal mean zonal winds at 2000 K potential temperature in the SH (Figure 3) suggests a strong and extended vortex in midwinter and a weakening of the vortex in mid-August. The reversal of the mean zonal winds from easterlies to westerlies indicate the final breakup of the vortex in October.

[15] Figure 4 (top) shows the temporal evolution of the vortex boundary position in equivalent latitudes. Until 15 May, the vortex edge was localized around 50–60°S. From June to the end of July, when the NO_x enhancements were most pronounced, the vortex above 1500 K was extended up to 30°S equivalent latitudes. With the weakening of the vortex in August, its latitudinal extension shrank again until its final breakup above 1500 K at the beginning of September. The apparent expansion of the polar vortex above 1700 K in September and October is produced by advection of the vortex tracers to the tropics after the final breakup.

[16] The temporal evolution of the total NO_x abundance averaged over the vortex area is presented in Figure 4 (middle). The pattern of the NO_x descent is very similar to that observed from the ESA NO_2 nighttime data. Maximum NO_x vortex averages of up to 60 ppbv were found at 3000 K in July. The vortex-averaged CO abundances (Figure 4, bottom) increased steadily until mid-Ma[illegible] of the descent [illegible]lated to the [illegible] enhanced mixing across the [illegible]. Descent rates of 400 m per day are derived from the CO isolines above 1500 K in May which is qualitatively consistent with typical wintertime descent rates in this altitude range [*Garcia and Solomon*, 1985]. Lower descent rates are derived from CH_4 (250 m per day). However, CH_4

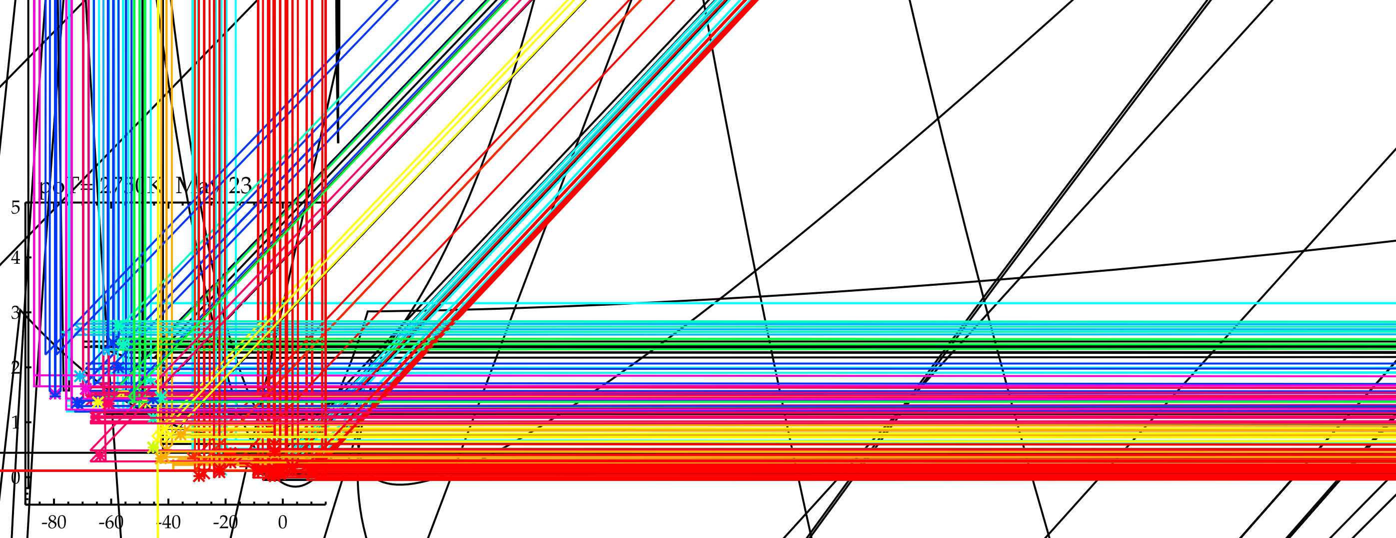

data could be affected by strong mixing below the subsidence zone leading to underestimated descent rates.

[17] The distribution of NO_x and CO inside the vortex at the 2500 K isentropic surface is shown in Figure 5 for days 9 June and 1 July along with ECMWF potential vorticity. High values of both NO_x and CO were confined to the vortex with sharp horizontal gradients at the edge. As expected, highest NO_x abundances were found in the polar night region with VMRs up to 8 times higher than in the illuminated part of the vortex. An opposite behavior is seen in the CO distributions which were more abundant in the outer part of the vortex, suggesting enhanced descent in the subpolar regions. Strong vertical transport close to the inner edge of the vortex boundary is also visible in Figure 2 (top), always showing the highest CO abundances close to the vortex boundary. Since the Eliassen-Palm flux divergence often peaks at midlatitudes in the SH [*Garcia et al.*, 1992], enhanced descent in the subpolar regions is not unusual. Potential vorticity had an isotropic distribution in the vortex boundary region and outside of the vortex. Inside the vortex, and most pronounced in the outer vortex region, however, potential vorticity was rather randomly distributed indicating strong turbulent mixing. This stirring process could have been responsible for the pronounced horizontal gradient in the NO_x VMR at the polar night terminator being slightly smoothed out on 1 July compared to 9 June. In fact, filaments of enhanced NO_x released from the polar night region showed up at around 150°E on both days. At altitudes above 50 km where NO photolysis is efficient, turbulent mixing inside the vortex could have contributed significantly to an accelerated NO_x loss by transporting NO_x to illuminated regions where it could be more easily destroyed.

[18] Figure 6 shows the measured NO_x distribution over equivalent latitude as 10° running mean for 8 days between 11 April and 31 August along with the vortex boundary.

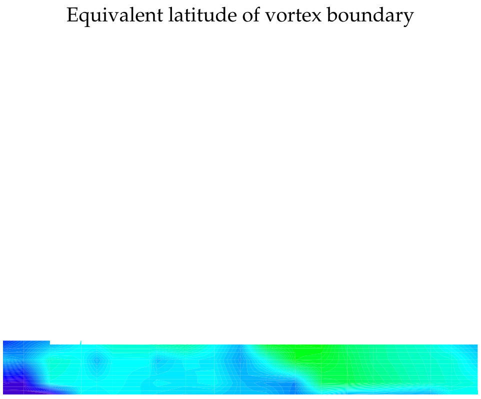

Single NO_x measurements and potential vorticity along equivalent latitude for potential temperature levels of 1000 K, 1750 K, and 2500 K are shown in Figure 7. As early as 11 April, a slight increase of 5 ppbv above 2500 K can be seen in the mean NO_x abundances close to the vortex core (Figure 6). Single measurements reached here values of 14 ppbv (Figure 7). Mean NO_x abundances increased to 15–20 ppbv by the end of April.

[19] On 17 May, apart of the enhancements at the vortex center, a second increase of the mean NO_x abundances shows up close to the vortex edge above 2000 K (Figure 6). This provides further evidence for a strong descent at the inner side of the vortex boundary. Highest NO_x abundances with mean values exceeding 150 ppbv were found on 9 June. Even at 1500 K, the mean NO_x VMR was around 100 ppbv. Peak VMRs of single measurements exceeded 200 ppbv (Figure 7). The abundance of NO_x decreased strongly toward the outer regions of the vortex as already seen in Figure 5. On 1 July, NO_x mean VMRs were smaller again, although more homogeneously distributed throughout the vortex. Since on this day the highest NO_x concentrations were still found in the polar night region (see Figure 5), the homogeneous distribution along equivalent latitudes demonstrates that potential vorticity was rather randomly distributed inside the vortex, i.e., vortex core and polar night region did not coincide. Enhanced turbulent mixing inside the vortex, smoothing out differences of the NO_x load inside and outside the polar night region, is evident in the distributions of single NO_x measurements on 1 July compared to 9 June above 1750 K (Figure 7). A high degree of confinement of the NO_x enhancements to the vortex area is clearly visible.

[20] On 21 July, and even more pronounced on 11 August, mean NO_x abundances were decreasing in the outer region of the vortex above 1500 K (see Figure 6). This could have been caused by either photochemical loss or by dilution due to NO_x-poor tropical air brought into the vortex. The first possibility seems to be unlikely since NO_x depletion was not more pronounced at higher altitudes, as one would expect in the case of photochemical loss. Furthermore, as shown in section 6, photochemical NO_x loss rates inside the vortex were in the order of 1% per day, much less than required to explain the observed decrease. The observed NO_x depletion is thus more likely caused by mixing across the vortex boundary. In the 1000–1500 K region, a tongue of enhanced NO_x moving out of the vortex might hint at a NO_x outflow on these two days. A flow of NO_x-rich upper atmospheric air out of the vortex at 1750 K and 2500 K can also be observed on 21 August in the bottommost plot of Figure 7.

[21] On 31 August, the pronounced horizontal gradients in the NO_x distribution at the vortex edge had disappeared above 1500 K indicating that the vortex was seriously weakened and did not act as a transport barrier anymore. Mean NO_x abundances above 1500 K decreased to approximately 10 ppbv which is close to the mixing ratio expected under undisturbed conditions. Below 1500 K, however, NO_x enhancements persisted and were confined to the vortex.

4. NO_x Sources

[22] In this section, possible sources for the NO_x enhancements in the Antarctic winter 2003 are discussed. It is of particular importance to clarify if in situ production due to energetic particle precipitation had contributed to the observed enhancements or if the NO_x was mainly produced in

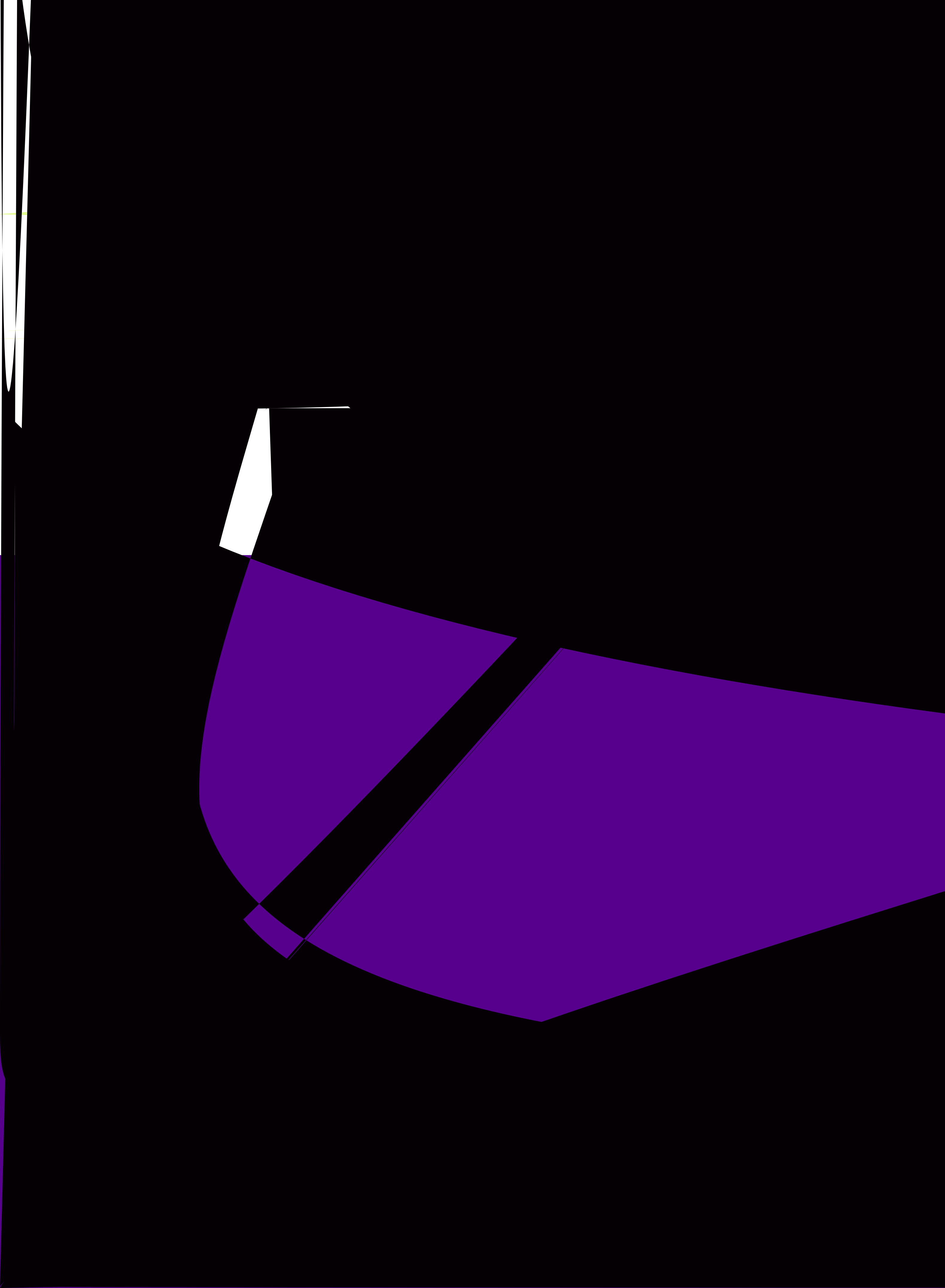

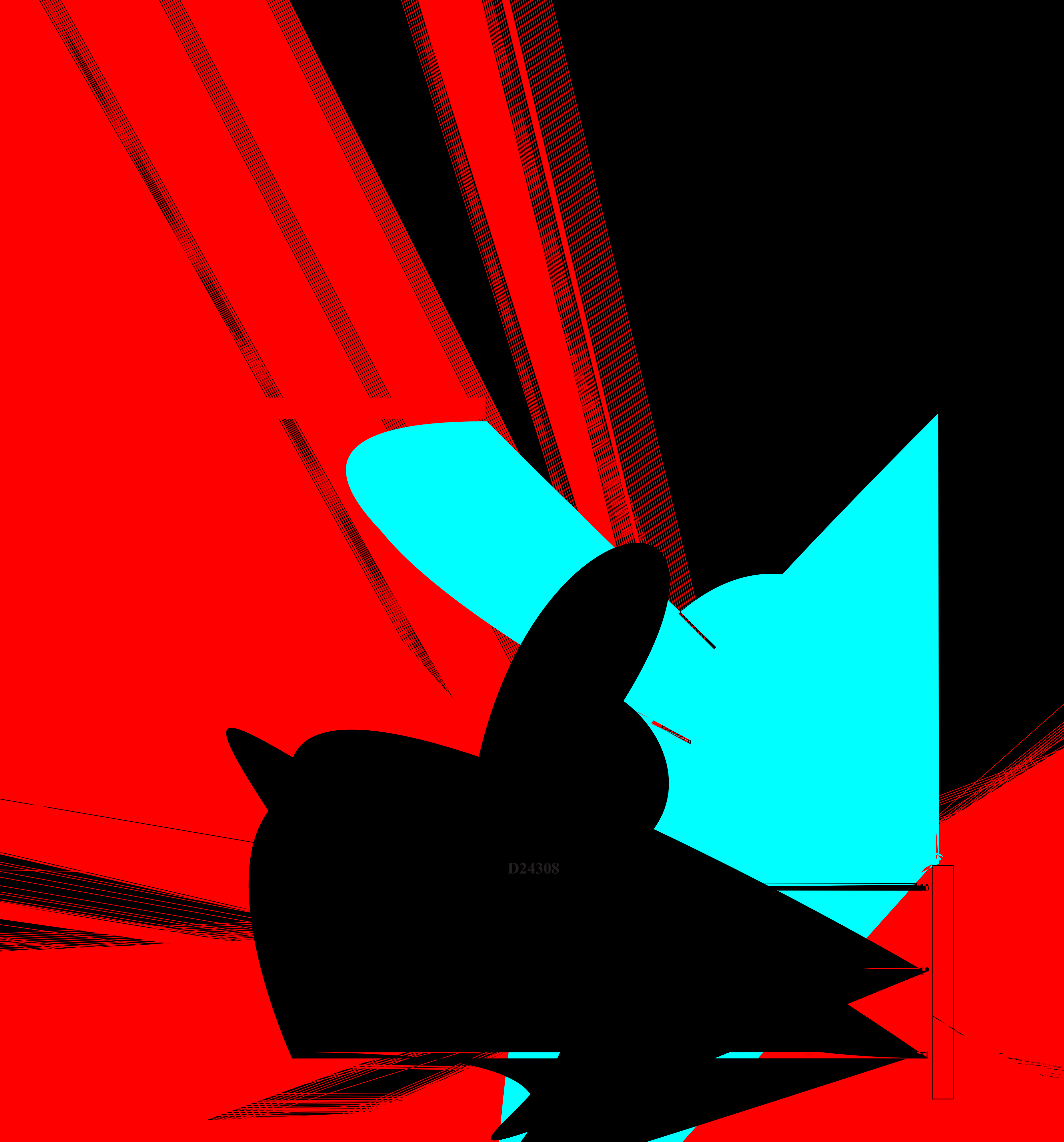

Figure 6. Potential temperature-equivalent latitude daily mean cross sections of NO_x VMR for the days 11 April, 29 April, 17 May, 9 June, 1 July, 21 July, 11 August, and 31 August 2003. The solid red line indicates the vortex edge. The vortex boundary region is shown by the dotted red lines around the edge. White regions indicate missing data. See Figure 4 for corresponding geometric altitudes.

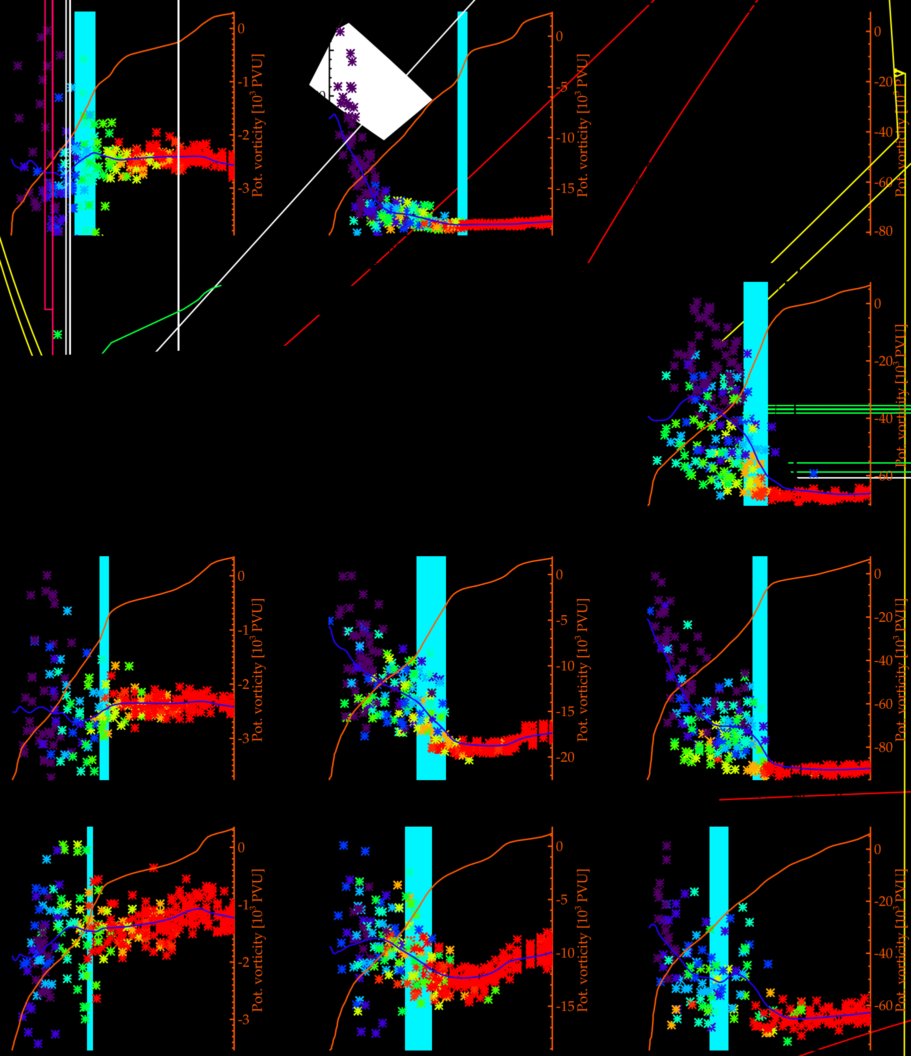

Figure 7

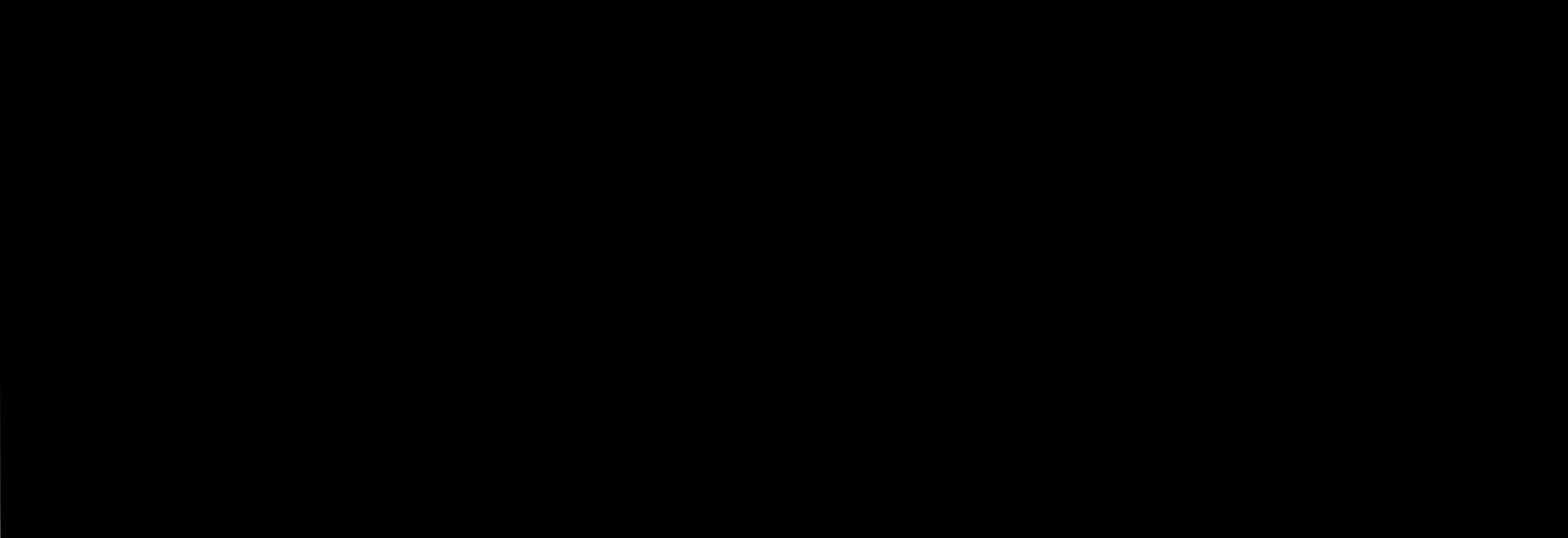

Figure 8. (top) Integral precipitating electron fluxes averaged over L > 2.5 and 60°–90

). (bottom) Abundances of nighttime NO2 (solid line) and CH4 (shaded line) from ESA data averaged over 60°–90° S equivalent

on the time axis correspo nd to days with available IMK/IAA data. ratio inside the vortex from IMK/IAA data (shaded dotted line with symbo

[redacted]

s
th
bec
[200
70 km
day at
Solomon,
ities of 0.8
region in July
while at 50 km,
300–500 m per
downward velocities
the temporal evolution
which is in agreement with
stratopause, however, descent ra
might be overestimated by mode
temperature measurements over the So
[*Pan and Gardner*, 2003].

[26] Horizontal transport processes affect the NO_x [redacted]
into the stratosphere by redistributing NO_x from the polar night area to illuminated regions where it is photochemically destroyed. The breaking of planetary waves accelerates horizontal mixing, increases the extension and permeability of the polar vortex, and determines the timing of the spring warming and the breakdown of the vortex. By inclusion of planetary wave forcing in model calculations of the NO_x descent during a typical Antarctic winter, *Siskind* [2000] achieved good agreement with HALOE observations above 60 km. In the lower mesosphere (50–60 km), however, an additional mixing term was required to reproduce the HALOE observations of high NO_x at midlatitudes. As discussed in section 3, MIPAS data give evidence for

[redacted]
their ma
in August/Septe
evolution of ECMWF zo
September 2003 (Figure 3).

6. Stratospheric NO_x Deposition

[29] The quantification of the amount of NO_x brought down into the stratosphere before being photolyzed is extremely important in order to assess the impact of upper atmospheric NO_x on stratospheric ozone chemistry. This amount was calculated by *Siskind* [2000] for a typical

ate

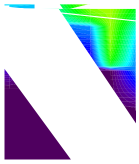

amounts modeled \
ric source. Under co.
and additional mixing
t was determined to be
mations of the strato-
E data [*Siskind et al.*,
f only 1 GM during
tron precipitation. This
ratospheric subcolumn
proximately 600 and
er. Within this altitude
of around 11 ppbv at
94. MIPAS NO_x shows
early October 2003 at
levels (1000 K). These
ence in 2003 compared
vious years. However,
r when integrating the
disagreement between
periments can only be
on of the upper atmo-
n of the dynamical or
and observed NO_x dis-
July, the disagreement
mation of transport out
te winter by the model.
ixing across the weak-
tratosphere reduces the
m, where it acts on the
However, NO_x trans-
km represents still an
heric NO_x on a global
far.
evolution of the total
de the vortex in the
re allows to estimate
ported downward from
polar winter, (2) the
n spring, and (3) the
he vortex at different
a offers an excellent
evolution since global
ustral winter 2003. By

integrating measured NO_x densities inside the vortex on isentropic surfaces and subsequently integrating over altitudes between potential temperatures of 625 K to 1250 K, 1250 K to 2000 K, and 2000 K to 3000 K, we have calculated total amounts of NO_x in three different regions. The lowest one, 625–1250 K, represents the part of the vortex which remains stable until mid-October. The lower boundary 625 K was chosen because CH_4 abundances at this level remain constant from July to October indicating that no further subsidence took place below. This altitude region is approximately the same as that chosen by *Siskind et al.* [2000] in order to estimate the upper atmospheric NO_x content of the SH polar vortex in spring. The 1250–2000 K region represents the part of the vortex which is weakened already in August but photochemical loss is not significant. Finally, the highest region accounts for the remaining altitudes up to the highest levels which has been measured.

[31] In order to account for photochemical losses, daily mean photochemical loss rates L_d at different potential temperature levels have been derived by time integration the NO loss rates due to photodissociation at the location each observation within 24 hours and subsequently ging these losses over the vortex area. Measurements w eighted with the number density at the considered alt and with cos(θ) to account for the variation of the repre ve surface of each measurement with latitude, θ. Solar angle–dependent NO photolysis rates have been calc using the parameterization of *Minschwaner and Siskin* 3]. It has been assumed that each photolysis event d s two NO molecules because of subsequent recomb of N and NO (R2). The calculated daily mean loss r re illustrated in Figure 10. At 3000 K, L_d varies between and 0.01 day^{-1} before August with a minimum in June. in the year, L_d increases up to 0.1 day^{-1} in October. At K, L_d stays below 0.002 day^{-1}, except for October. B 1500 K, values of L_d are negligible small. The amou photochemically destroyed NO_x accumulated until a g day within the altitude regions defined above was th alculated by integrating the product of L_d and the total N amount from 11 April until the day under consideration. and NO_x amounts between the days with data availab of IMK/IAA products have been linearly interpolated.

[32] To estimate the amount of upper nospheric NO_x deposited in the middle stratosphere, the co rsion of NO_x to NO_y reservoir gases has to be taken into ac nt. We thus add to the NO_x amounts measured at 625– 0 K and 1250–2000 K the amounts of HNO_3 and $2N_2O$ inferred from MIPAS data as described in a companion pape *Stiller et al.*, 2005]. Only the minor species $ClONO_2$, Br O_2, HNO_4, and NO_3, which do not significantly contribu in this altitude region, were not included in the NO_y budget. order to remove from the measured NO_y amounts the contribution which has no upper atmospheric origin, we subtract the values measured on 11 April for the 1250–2000 K and the 2000–3000 K regions. For the 625–1250 K region, the amount of NO_y measured on 1 July has been subtracted, assuming that on this day the upper atmospheric NO_x had not reached yet this altitude region while background NO_x and NO_y had already subsided. For NO_x, this assumption is justified from the temporal evolution shown in Figure 1. For the other NO_y species, Figure 4 of *Stiller et*

assumption is justifie
at the 3000 K (and a
Figure 10) which led
before the air reached
and second, vertical
decreased after the w

[34] The accu 3000 K
region during subtractin
from the to (3.1 GM)
NO_y a of the
(1.1 cumulat
ts dy
furth
regio
compe
dicati
they
e a
the C
een th
nd 10
Augu
aini
nam
belo
ca

[2 that the 1 July re
ckground
of upp

tion of th
O_x and O_y ob
t alt regions. Th
O photolysis converted into
ed separat The increasing
altitude re s the fact that
th altitude which led to an
s at r altitudes. The
day when NO_x amounts
maximi October an
The total a of
measured in
ed in maxim

2003 wh
amount stayed in the po
October and 5% was mixed out of t

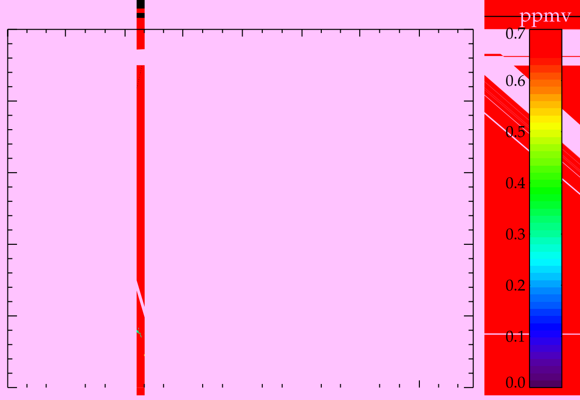

Figure 12. Temporal evolution of MIPAS (ESA data) (top) NO_2 and (bottom) CH_4 nighttime abundances averaged within 60°–90°N equivalent latitudes at isentropic surfaces from 625 K to 3000 K during Arctic winter 2002/2003. An area-weighting factor (cosine of latitude) has been applied. White regions indicate missing data or CH_4 abundances exceeding 0.7 ppmv.

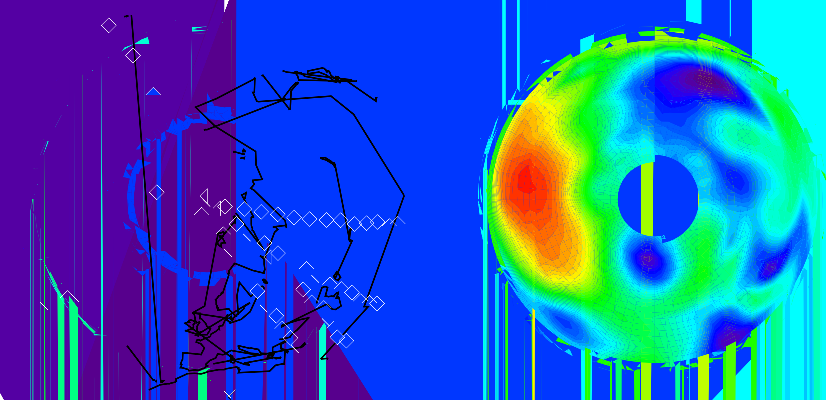

measu b
1979.
polar
winter
ments

[44]
nism
has
of
(1

of NO_x and CO inside the vortex on the isentropic surface of 2500 K in June and July.

[47] The total amount of NO_x injected into stratosphere without being photochemically destroyed has been estimated to be 2.4 GM. 1.1 GM of this amount remained in the polar vortex until the final warming in mid-October, while 1.3 GM were transported out of the vortex by isentropic mixing before. The amount of NO_x remaining inside of the SH vortex in late spring had been previously estimated from HALOE data to 0.8–1.3 GM [*Siskind et al.*, 2000] which is in good agreement with our results. The portion of NO_x transported out of the vortex represents a new source of NO_x to the stratosphere which thus doubles the previous estimates of the stratospheric NO_x deposition derived from HALOE data. Upper atmospheric NO_x contributes then to the total NO_y source in the stratosphere with 9% of the dominant N_2O oxidation source.

[48] No evidence for an unusual dynamical situation was found in the 2003 SH winter from the derived descent rates and from the temporal evolution and extension of the polar vortex. Taking into account that the dynamical conditions in the SH are generally less variable than in the NH, the NO_x descent in the Austral winter 2003 might be representative for the SH from the dynamical point of view. If so, the polar winter descent of upper atmospheric NO_x can have a significant impact on the stratospheric NO_y budget on a longer timescale and might explain the underestimation of NO_x at its VMR peak height by chemical transport models [*TOPOZ III*, 2005]. Since electron precipitation from the outer trapping region and auroral events as upper atmospheric NO_x production mechanisms are more frequent in the declining phase of the solar cycle [*Rangarajan and Barreto*, 2000], a solar cycle modulation of the upper atmospheric NO_x source with a phase lag of 2–3 years is expected. Because of the dynamical coupling of the upper atmosphere and the stratosphere, this modulation will affect stratospheric NO_y and O_3. Model calculations performed by *Callis et al.* [2001] indicate that the amplitude of the solar cycle modulation by electron precipitation of the global ozone column from 25 to 45 km could be in the order of 2.5%, nearly twice as much as the amplitude due to UV effects.

[49] NO_x and tracer distributions observed during several days in the NH winter 2002/2003 have also been analyzed. We found that high planetary wave activity resulting in the major midwinter warming led to a rather inefficient NO_x downward transport with negligible deposition of NO_x in the lower and middle stratosphere. Since major warming events in midwinter are a typical feature of the Northern Hemisphere, an insignificant NO_x deposition due to unfavorable dynamical conditions, as observed in the 2002/2003 winter, is expected to happen frequently. On the other hand, dynamical conditions in the NH winters are much more variable, resulting thus in a higher variability of the NO_x deposition. The MIPAS observations of NO_x in the NH winter 2003/2004 [*López-Puertas et al.*, 2005] with record values of around 350 ppbv detected in the strong polar vortex during February and March, demonstrate how drastically dynamical conditions and NO_x deposition can vary within two successive years in the NH. Although it might not be excluded that the October/November 2003 SPEs have contributed to the extraordinary NO_x enhancements detected in the upper stratosphere in early 2004, the bulk of descended NO_x was attributed to electron precipitation similar as in the Antarctic winter 2003 [*López-Puertas et al.*, 2005]. The net deposition of NO_x in the NH stratosphere in early 2004 is a topic of future work.

[50] **Acknowledgments.** The authors acknowledge ESA for providing MIPAS spectra and L2 data, as well as NILU and ECMWF for meteorological data. The IAA team has been supported by Spanish Ministerio de Educación y Ciencia under projects REN2001-3249/CLI and ESP2004–01556 and EC FEDER funds. The IMK team was supported by SACADA (BMBF 07ATF53) and by the EU-Project TOPOZ-III (EVK2-CT-2001-00102).

References

Callis, L. B., and J. D. Lambeth (1998), NO_y formed by precipitating electron events in 1991 and 1992: Descent into the stratosphere as observed by ISAMS, *Geophys. Res. Lett.*, *25*(11), 1875–1878.

Callis, L. B., M. Natarajan, D. S. Evans, and J. D. Lambeth (1998a), Solar-atmospheric coupling by electrons (SOLACE): 1. Effects of the May 12, 1997 solar event on the middle atmosphere, *J. Geophys. Res.*, *103*(D21), 28,405–28,419.

Callis, L. B., M. Natarajan, J. D. Lambeth, and D. N. Baker (1998b), Solar-atmospheric coupling by electrons (SOLACE): 2. Calculated stratospheric effects of precipitating electrons, 1979–1988, *J. Geophys. Res.*, *103*(D21), 28,421–28,438.

Callis, L. B., M. Natarajan, and J. D. Lambeth (2001), Solar-atmospheric coupling by electrons (SOLACE): 3. Comparisons of simulations and observations, 1979–1997, issues and implications, *J. Geophys. Res.*, *106*(D7), 7523–7539.

Callis, L. B., M. Natarajan, and J. D. Lambeth (2002), Observed and calculated NO, 1992–1997, *Geophys. Res. Lett.*, *29*(2), 1030, doi:10.1029/2001GL013995.

Carli, B., et al. (2004), First results of MIPAS/ENVISAT with operational Level 2 code, *Adv. Space Res.*, *33*(7), 1012–1019, doi:10.1016/S0273-1177(03)00584-2.

Dunkerton, T. J., and D. P. Delisi (1985), The subtropical mesospheric jet observed by the NIMBUS 7 Limb Infrared Monitor of the Stratosphere, *J. Geophys. Res.*, *90*, 10,681–10,692.

European Space Agency (2000), Envisat, MIPAS: An instrument for atmospheric chemistry and climate research, *Eur. Space Agency Spec. Publl. ESA SP-1229*.

Fischer, H., and H. Oelhaf (1996), Remote sensing of vertical profiles of atmospheric trace constituents with MIPAS limb-emission spectrometers, *Appl. Opt.*, *35*(16), 2787–2796.

Frederick, J. E., and N. Orsini (1982), The distribution and variability of mesospheric odd nitrogen: A theoretical investigation, *J. Atmos. Terr. Phys.*, *44*, 479–488.

Funke, B., M. López-Puertas, G. P. Stiller, T. von Clarmann, and M. Höpfner (2001), A new non–LTE retrieval method for atmospheric parameters from MIPAS–ENVISAT emission spectra, *Adv. Space Res.*, *27*(6–7), 1099–1104.

Funke, B., et al. (2003), Non–LTE retrieval of NO, NO_2, and CO from MIPAS–ENVISAT, paper presented at 11th International Workshop on Atmospheric Science from Space using Fourier Transform Spectrometry, Forsch. Karlsruhe, Inst. für Meteorol. und Klimaforsch., Bad Wildbad, Germany, 8–10 Oct.

Funke, B., et al. (2005), Retrieval of stratospheric NO_x from 5.3 and 6.2 μm nonlocal thermodynamic equilibrium emissions measured by Michelson Interferometer for Passive Atmospheric Sounding (MIPAS) on Envisat, *J. Geophys. Res.*, *110*, D09302, doi:10.1029/2004JD005225.

Garcia, R. R., and S. Solomon (1985), The effect of breaking gravity waves on the dynamics and chemical composition of the mesosphere and lower thermosphere, *J. Geophys. Res.*, *90*, 3850–3868.

Garcia, R. R., and S. Solomon (1994), A new numerical model for the middle atmosphere: 2. Ozone and related species, *J. Geophys. Res.*, *99*, 12,937–12,951.

Garcia, R. R., F. Stordal, S. Solomon, and J. T. Kiehl (1992), A new numerical model for the middle atmosphere: 1. Dynamics and transport of tropospheric source gases, *J. Geophys. Res.*, *97*, 12,967–12,991.

Glatthor, N., et al. (2005), Mixing processes during the Antarctic vortex split in September/October 2002 as inferred from source gas and ozone distributions from MIPAS/ENVISAT, *J. Atmos. Sci.*, *62*(3), 787–800.

Harvey, V. L., R. B. Pierce, T. D. Fairlie, and M. H. Hitchman (2002), A climatology of stratospheric polar vortices and anticyclones, *J. Geophys. Res.*, *107*(D20), 4442, doi:10.1029/2001JD001471.

Jackman, C. H., and R. D. McPeters (2004), The effect of solar proton events on ozone and other constituents, in *Solar Variability and Its Effect on Climate*, *Geophys. Monogr. Ser.*, vol. 141, edited by J. M. Pap and P. Fox, pp. 305–319, AGU, Washington, D. C.

Jackman, C. H., R. D. McPeters, G. J. Labow, E. L. Fleming, C. J. Praderas, and J. M. Russell (2001), Northern Hemisphere atmospheric effects due to the July 2000 solar proton event, *Geophys. Res. Lett.*, *28*(15), 2883–2886.

López-Puertas, M., B. Funke, S. Gil-López, T. von Clarmann, G. P. Stiller, S. Kellamnn, H. Fischer, and C. H. Jackman (2005), Observation of NO_x enhancements and ozone depletion in the Northern and Southern hemispheres after the October–November 2003 solar proton events, *J. Geophys. Res.*, *110*, A09S43, doi:10.1029/2005JA011050.

Manney, G. L., J. L. Sabutis, D. R. Allen, W. A. Lahoz, A. A. Scaife, C. E. Randall, S. Pawson, R. Swinbank, and B. Naujokat (2005), Simulations of dynamics and transport during the September 2002 Antarctic major warming, *J. Atmos. Sci.*, *62*(3), 690–707.

Minschwaner, K., and E. Siskind (1993), A new calculation of nitric oxide photolysis in the stratosphere, mesosphere, and lower thermosphere, *J. Geophys. Res.*, *98*(D11), 20,401–20,412.

Nash, E. R., P. A. Newmann, J. E. Rosenfield, and M. R. Schoeberl (1996), An objective determination of the polar vortex using Ertel's potential vorticity, *J. Geophys. Res.*, *101*(D5), 9471–9478.

Nett, H., B. Carli, M. Carlotti, A. Dudhia, H. Fischer, J.-M. Flaud, G. Perron, P. Raspollini, and M. Ridolfi (1999), MIPAS ground processor and data products, paper presented at 1999 International Geoscience and Remote Sensing Symposium, Inst. of Electr. and Electron. Eng., Hamburg, Germany, 28 June–2 July.

Norton, H., and R. Beer (1976), New apodizing functions for Fourier spectrometry, *J. Opt. Soc. Am.*, *66*(3), 259–264. (Errata, *J. Opt. Soc. Am.*, *67*, 419, 1977.)

Pan, W., and C. S. Gardner (2003), Seasonal variations of the atmospheric temperature structure at South Pole, *J. Geophys. Res.*, *108*(D18), 4564, doi:10.1029/2002JD003217.

Randall, C. E., D. W. Rusch, R. M. Bevilacqua, K. W. Hoppel, and J. D. Lumpe (1998), Polar ozone and aerosol measurement (POAM) II stratospheric NO_2, 1993–1996, *J. Geophys. Res.*, *103*(D21), 28,361–28,371.

Rangarajan, G., and L. M. Barreto (2000), Long term variability in solar wind velocity and IMF intensity and the relationship between solar wind parameters and geomagnetic activity, *Earth Planets Space*, *52*, 121–132.

Ridolfi, M., et al. (2000), Optimized forward and retrieval scheme for MIPAS near-real-time data processing, *Appl. Opt.*, *39*(8), 1323–1340.

Rinsland, C. P., et al. (1999), Polar stratospheric descent of NO*y* and CO and Arctic denitrification during winter 1992–1993, *J. Geophys. Res.*, *104*(D1), 1847–1861.

Russell, J. M., III, C. Farmer, C. Rinsland, R. Zander, L. Froidevaux, G. Toon, B. Gao, J. Shaw, and M. Gunson (1988), Measurements of odd nitrogen compounds in the stratosphere by the ATMOS experiment on Spacelab 3, *J. Geophys. Res.*, *93*(D2), 1718–1736.

Siskind, D. E. (2000), On the coupling between middle and upper atmospheric odd nitrogen, in *Atmospheric Science Across the Stratopause*, *Geophys. Monogr. Ser.*, vol. 123, edited by D. E. Siskind, S. D. Eckermann, and M. E. Summers, pp. 101–116, AGU, Washington, D. C.

Siskind, D. E., J. T. Bacmeister, M. E. Summers, and J. M. Russell III (1997), Two–dimensional model calculations of nitric oxide transport in the middle atmosphere and comparison with Halogen Occultation Experiment data, *J. Geophys. Res.*, *102*(D3), 3527–3545.

Siskind, D. E., G. E. Nedoluha, C. E. Randall, M. Fromm, and J. M. Russell III (2000), An assessment of Southern Hemisphere stratospheric NO_x enhancements due to transport from the upper atmosphere, *Geophys. Res. Lett.*, *27*, 329–332.

Solomon, S., P. J. Crutzen, and R. G. Roble (1982), Photochemical coupling of the thermosphere and the lower atmosphere: 1. Odd nitrogen from 50 to 120 km, *J. Geophys. Res.*, *87*, 7206–7220.

Stiller, G. P., et al. (2005), An enhanced HNO_3 second maximum in the Antarctic mid-winter upper stratopshere, *J. Geophys. Res.*, *110*, D20303, doi:10.1029/2005JD006011.

TOPOZ III (2005), Towards the prediction of stratospheric ozone III, *Final Rep., Contract EVK2-CT-2001-00102*, Eur. Comm., Brussels.

von Clarmann, T., et al. (2003a), Retrieval of temperature and tangent altitude pointing from limb emission spectra recorded from space by the Michelson Interferometer for Passive Atmospheric Sounding (MIPAS), *J. Geophys. Res.*, *108*(D23), 4736, doi:10.1029/2003JD003602.

von Clarmann, T., et al. (2003b), Remote sensing of the middle atmosphere with MIPAS, in *Remote Sensing of Clouds and the Atmosphere VII*, vol. 4882, edited by K. Schäfer et al., pp. 172–183, SPIE–Int. Soc. for Opt. Eng., Bellingham, Wash.

H. Fischer, S. Kellmann, G. P. Stiller, and T. von Clarmann, Forschungszentrum Karlsruhe und Universität Karlsruhe, Institut für Meteorologie und Klimaforschung, Postfach 3640, D-76021 Karlsruhe, Germany.

B. Funke, S. Gil-López, and M. López-Puertas, Instituto de Astrofísica de Andalucía, Apartado Postal 3004, E-18080 Granada, Spain. (bernd@iaa.es)